



HAL
open science

Variance computation of the Modal Assurance Criterion

Szymon Gres, Michael Dohler, Palle Andersen, Laurent Mevel

► **To cite this version:**

Szymon Gres, Michael Dohler, Palle Andersen, Laurent Mevel. Variance computation of the Modal Assurance Criterion. ISMA 2018, 28th Conference on Noise and Vibration Engineering, Sep 2018, Leuven, Belgium. 12 p. hal-01886642

HAL Id: hal-01886642

<https://inria.hal.science/hal-01886642>

Submitted on 3 Oct 2018

HAL is a multi-disciplinary open access archive for the deposit and dissemination of scientific research documents, whether they are published or not. The documents may come from teaching and research institutions in France or abroad, or from public or private research centers.

L'archive ouverte pluridisciplinaire **HAL**, est destinée au dépôt et à la diffusion de documents scientifiques de niveau recherche, publiés ou non, émanant des établissements d'enseignement et de recherche français ou étrangers, des laboratoires publics ou privés.

Variance computation of the Modal Assurance Criterion

S. Gres¹, M. Döhler², P. Andersen³, L. Mevel²

¹ Aalborg University, Department of Civil and Structural Engineering,
Thomas Manns Vej 23, 9000 Aalborg, Denmark

² INRIA, University of Rennes, IFSTTAR/COSYS/SII, I4S
Campus de Beaulieu, 35042 Rennes, France

³ Structural Vibration Solutions A/S,
NOVI Science Park, 9220 Aalborg, Denmark

Abstract

Modal validation is an integral part of any modal analysis scheme. Recent advances in efficient variance computation of modal parameter estimates from the output-only subspace-based identification algorithms made the computation of variance feasible for the modal parameters, such as natural frequencies, damping ratios and mode shapes. One of the other practical modal indicators is Modal Assurance Criterion (MAC), for which uncertainty computation scheme is missing. This paper builds on the previous results using the propagation of the measurement uncertainties to estimates of MAC. The sensitivity of the MAC with respect to output covariances is derived using a first order perturbations and the uncertainties are propagated using the Delta method. The influence of the underlying mode shape scaling on both the uncertainty of mode shapes and MAC is investigated. The results are presented in context of operational modal analysis (OMA) of a spring mass system.

1 Introduction

Noisy vibration measurements deployed for the modal identification call to appreciate the statistical uncertainties due to the unknown nature of the input, limited sample size and sensor noise that inherently affect the estimated parameters. A general framework to evaluate the variance of the modal parameters has been proposed first for the covariance driven subspace identification in [7]. As such that strategy involves propagation of the sample covariance through the sequence of system identification steps based on sensitivity analysis where the analytical sensitivities are derived using a first order perturbation. This was revised with an efficient implementation of the latter for the multi-order [4] and multi-setup [2] identification scenarios. The propagation of the sample covariance for the output-only data driven algorithms has been established through a link between the sensitivity of the covariance Hankel matrix to its data driven counterpart [6]. Consequently, this development has led the variance to become a practical modal information, amongst a few others, for industrial applications of the subspace-based system identification.

Once identified from the eigenstructure of the state transition matrix, natural frequencies, damping ratios and mode shapes are validated with simple metrics like variance or relative errors between the estimates from different model orders in a stabilization diagram. When it comes to the mode shapes some additional indicators are commonly used; one of them is MAC. MAC value is a real scalar bounded by zero and one, which depicts a degree of colinearity between two mode shape vectors [5]. In practice, it is a useful tool to assess the quality of conducted modal identification or cross correlate results between different modal tests, however, like estimates of the modal parameters, MAC is affected by the measurement uncertainties.

MAC can be deployed for the comparison of two mode shapes estimated from a single model order, between

different model orders, between two global model orders, between different data sets and lastly between the mode shape extracted from the finite element model and the mode shape estimated from the data collected from the corresponding structure. A strategy to propagate the mode shape covariance estimated from an arbitrary subspace identification algorithm to MAC estimated between different mode shapes is the subject of the present paper. Different mode shape normalization schemes are recalled in the next section. In Section 3 the analytical sensitivity of MAC is derived and Section 4 contains the results of the uncertainty quantification of the numerical simulations of a chain-like system both in the proposed and Monte Carlo frameworks.

2 Subspace system identification

Let model (1) represent a behavior of a d degree of freedom, viscously damped, linear time-invariant (LTI) structural system,

$$\begin{cases} M\ddot{u}(t) + D\dot{u}(t) + Ku(t) = v(t) \\ y(t) = C_a\ddot{u} + C_v\dot{u}(t) + C_d u(t) \end{cases} \quad (1)$$

where $y(t) \in \mathbb{R}^r$ is the output vector and (\cdot) expresses a derivative with respect to time t . Matrices $K, M, D \in \mathbb{R}^{d \times d}$ denote stiffness, mass and damping matrices respectively. Matrices $C_a, C_v, C_d \in \mathbb{R}^{r \times d}$ are selection matrices for accelerations, velocities and displacements where r is the number of sensors. Vectors $u(t), v(t) \in \mathbb{R}^d$ denote the continuous-time displacements and external forces respectively. Sampled with k discrete steps at rate $1/\tau$, System (1) can be represented with a discrete-time stochastic state-space model

$$\begin{cases} x_{k+1} = A_n x_k + w_k \\ y_k = C_n x_k + v_k \end{cases} \quad (2)$$

where $x_k \in \mathbb{R}^n$ are the states; $A_n \in \mathbb{R}^{n \times n}$, $C_n \in \mathbb{R}^{r \times n}$ are the state transition and observation matrices estimated for a model order n and vectors w_k with v_k denote the process and output noises respectively. The eigenfrequencies f_i , damping ratios ζ_i and mode shapes φ_i of the underlying mechanical system (1) are identified for $i = 1 \dots n$ from the i -th eigenvalue λ_i and eigenvector Φ_i of A_n such that

$$f_i = \frac{|\lambda_{ci}|}{2\pi}, \quad \zeta_i = \frac{-\Re(\lambda_{ci})}{|\lambda_{ci}|}, \quad \varphi_i = C_n \Phi_i \quad (3)$$

where the eigenvalue of the continuous system λ_{ci} is computed with $e^{\lambda_{ci}\tau} = \lambda_i$. The $|\cdot|$ denotes modulus operator and $\Re(\cdot)$ and $\Im(\cdot)$ express real and imaginary parts of a complex variable. An example of an output-only data-driven identification algorithm, namely Stochastic Subspace Identification with Unweighted Principal Component, SSI-UPC, is given in the next paragraph.

2.1 SSI-UPC identification algorithm

The UPC algorithm is based on a projection of the ‘future’ data horizon \mathcal{Y}^+ onto the ‘past’ data horizon \mathcal{Y}^- , which associates the column space of the resulting projection matrix \mathcal{H} with the column space of the extended observability matrix Γ whereas its rows space corresponds to the row space of the forward Kalman filter state sequence X . The projection can be written as

$$\mathcal{H} = \mathcal{Y}^+ / \mathcal{Y}^- = \mathcal{Y}^+ \mathcal{Y}^{-T} (\mathcal{Y}^- \mathcal{Y}^{-T})^{-1} \mathcal{Y}^- \quad (4)$$

where $\mathcal{H} \in \mathbb{R}^{(p+1)r \times N}$ with $N + p + q$ denoting the total number of samples such that parameters p, q are usually $p = q + 1$. Matrices $\mathcal{Y}^+ \in \mathbb{R}^{(p+1)r \times N}$ and $\mathcal{Y}^- \in \mathbb{R}^{qr_0 \times N}$ are defined such that

$$\mathcal{Y}^+ = \frac{1}{\sqrt{N}} \begin{bmatrix} y_{q+1} & y_{q+2} & \vdots & y_{N+q} \\ y_{q+2} & y_{q+3} & \vdots & y_{N+q+1} \\ \vdots & \vdots & \vdots & \vdots \\ y_{p+q+1} & y_{p+q+2} & \vdots & y_{p+q+N} \end{bmatrix}, \quad \mathcal{Y}^- = \frac{1}{\sqrt{N}} \begin{bmatrix} y_q^{r_0} & y_{q+1}^{r_0} & \vdots & y_{N+q-1}^{r_0} \\ y_{q-1}^{r_0} & y_q^{r_0} & \vdots & y_{N+q-2}^{r_0} \\ \vdots & \vdots & \vdots & \vdots \\ y_1^{r_0} & y_2^{r_0} & \vdots & y_N^{r_0} \end{bmatrix}$$

with r_0 labeling the reference channels. An efficient and numerically stable scheme to compute the Hankel matrix \mathcal{H} has been proposed in [9] and [3]. Instead of the direct computation of the projection as in (4), it involves selecting an appropriate partition of the stacked and LQ decomposed \mathcal{Y}^- and \mathcal{Y}^+ matrices.

Matrix \mathcal{H} enjoys the factorization property into $\mathcal{H} \approx \Gamma_n X_n$ where $\Gamma_n \in \mathbb{R}^{(p+1)r \times n}$ and $X_n \in \mathbb{R}^{n \times N}$ are defined as

$$\Gamma_n = \begin{bmatrix} C_n \\ C_n A_n \\ \vdots \\ C_n A_n^p \end{bmatrix}, \quad X_n = [G_n \quad A_n G_n \quad \dots \quad A_n^{q-1} G_n] \Sigma_{\mathcal{Y}^-}^{-1} \mathcal{Y}^- \quad (5)$$

where $G_n = \mathbb{E}(x_{k+1} y_k^T)$ expresses the cross covariance computed between the states at model order n and the outputs, and the matrix $\Sigma_{\mathcal{Y}^-} = \mathbb{E}((\mathcal{Y}^- \mathcal{Y}^{-T}))$ is the variance of \mathcal{Y}^- . In practice, only the estimates of the observability matrix $\hat{\Gamma}_n$ and the forward Kalman states \hat{X}_n are computed. A well-known scheme to compute $\hat{\Gamma}_n$ and \hat{X}_n is to balance the singular values of the estimate of the Hankel matrix, $\hat{\mathcal{H}}$, which SVD writes

$$\hat{\mathcal{H}} = [U_1 \quad U_2] \begin{bmatrix} D_1 & 0 \\ 0 & D_2 \end{bmatrix} \begin{bmatrix} V_1^T \\ V_2^T \end{bmatrix} \quad (6)$$

where $\hat{\Gamma}_n = U_1 D_1^{1/2}$ and $\hat{X}_n = D_1^{1/2} V_1^T$. U_1 and V_1 are the left and right singular vectors corresponding to first n non-zero singular values D_1 and U_2 with V_2 are the left and right kernel of $\hat{\mathcal{H}}$ where $D_2 \rightarrow 0$. The estimate of the state transition matrix A_n for a single model order can be computed in a least-square sense from the shift invariance property of $\hat{\Gamma}_n$ such that $\hat{A}_n = \hat{\Gamma}_n^\dagger \hat{\Gamma}_n^\downarrow$ and \hat{C}_n is extracted directly from the first block rows of $\hat{\Gamma}_n$. An efficient multi-model order scheme for the computation of the system matrices was developed in [3]. The modal parameter estimation follows (3).

2.2 Mode shape normalization

The mode shape φ_i computed from (3) is called the unnormalized mode shape since its scaling is arbitrary and its components can be written as $\varphi_i = [\varphi_{i,1} \quad \varphi_{i,2} \quad \dots \quad \varphi_{i,r}]^T$. To make it comparable between different model orders, a normalization scheme is needed. Two well-known schemes are investigated, namely

1. One mode shape component is set to 1. This k -th component can e.g. be chosen as the component with the maximum amplitude ($k = \arg \max_j \{|\varphi_{i,j}|\}$), or any other selected entry of φ_i . The normalized mode shape can be written as

$$\tilde{\varphi}_i = \varphi_i / \varphi_{i,k}. \quad (7)$$

Note that the k -th component in this normalized mode shape has, by design, no uncertainty.

2. The mode shape is rotated such that the imaginary part of one component is 0 and the real part of this component is positive. This k -th component can be chosen as in case 1. Then the mode shape is

rotated to the maximum angle of deflection. In addition, the norm of the mode shape is set to 1. Then, the normalized mode shape can be written as

$$\check{\varphi}_i = \tilde{\varphi}_i / \|\tilde{\varphi}_i\|. \quad (8)$$

Note that the imaginary part of the k -th component in this normalized mode shape has, by design, no uncertainty.

Note that the MAC value, see (13), is independent of the chosen mode shape normalization, therefore its uncertainty should also be independent of the chosen normalization scheme. Both schemes are investigated in this paper for the analysis of the mode shape uncertainty.

3 Delta method for variance estimation

Assume \hat{Y} to be a random matrix computed on N samples for which, as N goes to infinity, \hat{Y} converges almost surely to θ and the Central Limit Theorem, CLT, holds $\sqrt{N}(\hat{Y} - \theta) \xrightarrow{\mathcal{L}} \mathcal{N}(0, \text{cov}(\theta))$. This is e.g. the case for the output auto-covariance estimates computed from the measurements. Let $\text{vec}(\cdot)$ denote vectorization operator and $\text{vec}(X) = \text{vec}(f(Y))$ be once differentiable in θ with a sensitivity matrix $\mathcal{J}_{X,Y} = \left. \partial \text{vec}(f(Y)) / \partial \text{vec}(Y) \right|_{Y=\theta}$. The CLT formulated for \hat{X} writes as

$$\sqrt{N} \left(\text{vec}(\hat{X}) - \text{vec}(f(\theta)) \right) \xrightarrow{\mathcal{L}} \mathcal{N}(0, \mathcal{J}_{X,Y} \text{cov}(\theta) \mathcal{J}_{X,Y}^T) \quad (9)$$

and the first order perturbation of X can be written as $\text{vec}(\Delta X) = \mathcal{J}_{X,Y} \text{vec}(\Delta Y)$. The covariance of the estimate \hat{X} yields $\text{cov}(\text{vec}(\hat{X})) = \hat{\mathcal{J}}_{X,Y} \text{cov}(\text{vec}(\hat{Y})) \hat{\mathcal{J}}_{X,Y}^T$. In this way the covariance related to the output covariances in the Hankel matrix can be propagated to some function of it, in particular to the modal parameters and the MAC values. For the convenience of the notation the estimate symbol ($\hat{\cdot}$) is dropped in the next sections.

3.1 Variance of the mode shapes

The variance of the mode shapes is developed with respect to auto-covariance matrices of the measurements. The scheme in (10) follows the SSI-UPC algorithm developed in [1] and [6], here, for a single model order n . The first order perturbation of the mode shape $\Delta\varphi_i$ follows

$$\Delta\varphi_i = \mathcal{J}_{\varphi_i, (A_n, C_n)} \mathcal{J}_{(A_n, C_n), \Gamma_n} \mathcal{J}_{\Gamma_n, \mathcal{H}} \mathcal{J}_{\mathcal{H}, \mathcal{R}} \text{vec}(\Delta\mathcal{R}) \quad (10)$$

where $\mathcal{J}_{\varphi_i, (A_n, C_n)}$ is the sensitivity of the mode shape components with respect to the state transition and observation matrix computed at model order n , $\mathcal{J}_{(A_n, C_n), \Gamma}$ is the sensitivity of the state transition and observation matrix at model order n towards the observability matrix at order n , $\mathcal{J}_{\Gamma_n, \mathcal{H}}$ is the sensitivity of the observability matrix truncated at order n towards Hankel matrix and finally $\mathcal{J}_{\mathcal{H}, \mathcal{R}}$ is the sensitivity of the Hankel matrix towards the auto-covariance matrices of the measurements. The auto-covariance matrices $\text{vec}(\Delta\mathcal{R}) = \begin{bmatrix} \text{vec}(\Delta\mathcal{R}_+) \\ \text{vec}(\Delta\mathcal{R}_-) \end{bmatrix}$ where \mathcal{R}_+ and \mathcal{R}_- are respectively the mean of the auto-covariance of each block of the past and future measurements. To easen the notation, the following perturbations can be written as

$$\Delta\varphi_i = \mathcal{J}_{\varphi_i, \mathcal{R}} \text{vec}(\Delta\mathcal{R})$$

where $\mathcal{J}_{\varphi_i, \mathcal{R}} = \mathcal{J}_{\varphi_i, (A_n, C_n)} \mathcal{J}_{(A_n, C_n), \Gamma_n} \mathcal{J}_{\Gamma_n, \mathcal{H}} \mathcal{J}_{\mathcal{H}, \mathcal{R}}$ is the chained sensitivity of the i -th mode shape towards the auto-covariance matrices of the measurements.

3.1.1 Uncertainty of normalized mode shape: normalization 1

To compute the variance of the normalized mode shape, the effect of the normalization must be accounted for. The first order perturbation of the first normalization scheme, which was developed in [7], writes as

$$\begin{aligned}\Delta\tilde{\varphi}_i &= \Delta\left(\frac{1}{\varphi_{i,k}}\right)\varphi_i + \frac{1}{\varphi_{i,k}}\Delta\varphi_i \\ &= -\frac{1}{\varphi_{i,k}^2}\Delta(\varphi_{i,k})\varphi_i + \frac{1}{\varphi_{i,k}}\Delta\varphi_i \\ &= \frac{1}{\varphi_{i,k}}\underbrace{\left(-\frac{1}{\varphi_{i,k}}\varphi_i e_k^T + I_r\right)}_{=\mathcal{J}_{\tilde{\varphi}_i,\varphi_i}}\Delta\varphi_i,\end{aligned}$$

using the fact that the (scalar) $\varphi_{i,k} = e_k^T \varphi_i$ where e_k is the k -th unit vector. The respective covariance of the real and imaginary mode shape part writes thus

$$\text{cov}\left(\begin{bmatrix} \Re(\tilde{\varphi}_i) \\ \Im(\tilde{\varphi}_i) \end{bmatrix}\right) = \begin{bmatrix} \Re(\mathcal{J}_{\tilde{\varphi}_i,\varphi_i} \mathcal{J}_{\varphi_i,\mathcal{R}}) \\ \Im(\mathcal{J}_{\tilde{\varphi}_i,\varphi_i} \mathcal{J}_{\varphi_i,\mathcal{R}}) \end{bmatrix} \Sigma_{\mathcal{R}} \begin{bmatrix} \Re(\mathcal{J}_{\tilde{\varphi}_i,\varphi_i} \mathcal{J}_{\varphi_i,\mathcal{R}}) \\ \Im(\mathcal{J}_{\tilde{\varphi}_i,\varphi_i} \mathcal{J}_{\varphi_i,\mathcal{R}}) \end{bmatrix}^T. \quad (11)$$

where $\Sigma_{\mathcal{R}}$ can be easily estimated as a sample covariance on blocks of the data as in [1] and [6].

3.1.2 Uncertainty of normalized mode shape: normalization 2

Regarding the second normalization scheme depicted in (8), the first order perturbation of $\check{\varphi}_i$ writes as

$$\begin{aligned}\Delta\check{\varphi}_i &= \Delta\left(\frac{1}{\|\tilde{\varphi}_i\|}\right)\tilde{\varphi}_i + \frac{1}{\|\tilde{\varphi}_i\|}\Delta\tilde{\varphi}_i \\ &= -\frac{\tilde{\varphi}_i}{2\|\tilde{\varphi}_i\|^3}\Delta(\|\tilde{\varphi}_i\|^2) + \frac{1}{\|\tilde{\varphi}_i\|}\Delta\tilde{\varphi}_i \\ &= -\frac{\tilde{\varphi}_i}{\|\tilde{\varphi}_i\|^3}\Re(\tilde{\varphi}_i^H \Delta\tilde{\varphi}_i) + \frac{1}{\|\tilde{\varphi}_i\|}\Delta\tilde{\varphi}_i \\ &= \frac{1}{\|\tilde{\varphi}_i\|}\underbrace{\left(-\frac{\tilde{\varphi}_i}{\|\tilde{\varphi}_i\|^2}\Re(\tilde{\varphi}_i^H \mathcal{J}_{\tilde{\varphi}_i,\varphi_i} \mathcal{J}_{\varphi_i,\mathcal{R}}) + \mathcal{J}_{\tilde{\varphi}_i,\varphi_i} \mathcal{J}_{\varphi_i,\mathcal{R}}\right)}_{=\mathcal{J}_{\check{\varphi}_i,\mathcal{R}}}\text{vec}(\Delta\mathcal{R}),\end{aligned}$$

and thus for the covariance of the real and imaginary mode shape parts

$$\text{cov}\left(\begin{bmatrix} \Re(\check{\varphi}_i) \\ \Im(\check{\varphi}_i) \end{bmatrix}\right) = \begin{bmatrix} \Re(\mathcal{J}_{\check{\varphi}_i,\mathcal{R}}) \\ \Im(\mathcal{J}_{\check{\varphi}_i,\mathcal{R}}) \end{bmatrix} \Sigma_{\mathcal{R}} \begin{bmatrix} \Re(\mathcal{J}_{\check{\varphi}_i,\mathcal{R}}) \\ \Im(\mathcal{J}_{\check{\varphi}_i,\mathcal{R}}) \end{bmatrix}^T. \quad (12)$$

3.2 Uncertainty of MAC

The computation of MAC between two complex valued mode shapes vectors φ and ψ estimated at model order n follows [5] and writes

$$\text{MAC} = \frac{|\varphi^H \psi|^2}{\varphi^H \varphi \psi^H \psi} = \frac{\varphi^H \psi \psi^H \varphi}{\varphi^H \varphi \psi^H \psi} \quad (13)$$

Two general cases for the MAC computation are distinguished namely, first when φ and ψ are estimates of a different mode shape, hereby denoted as cross-MAC, and second when $\varphi = \psi$ are the same mode shape estimate, denoted as auto-MAC. Note that auto-MAC yields

$$\text{MAC} = \frac{|\psi^H \psi|^2}{\psi^H \psi \psi^H \psi} = \frac{\psi^H \psi \psi^H \psi}{\psi^H \psi \psi^H \psi} = 1, \quad (14)$$

and has no uncertainty. To quantify the uncertainty of cross-MAC, the aim is to obtain the first order perturbation of (13) with respect to the real and the imaginary parts of the mode shape vectors, which writes as

$$\Delta \text{MAC} = \underbrace{\begin{bmatrix} \frac{\partial \text{MAC}}{\partial \Re(\varphi)} & \frac{\partial \text{MAC}}{\partial \Im(\varphi)} & \frac{\partial \text{MAC}}{\partial \Re(\psi)} & \frac{\partial \text{MAC}}{\partial \Im(\psi)} \end{bmatrix}}_{=\mathcal{J}_{\text{MAC},\varphi,\psi}} \begin{bmatrix} \Delta \Re(\varphi) \\ \Delta \Im(\varphi) \\ \Delta \Re(\psi) \\ \Delta \Im(\psi) \end{bmatrix} \quad (15)$$

where the covariance of the MAC can be expressed in terms of the covariance of the mode shapes and the analytical sensitivity $\mathcal{J}_{\text{MAC},\varphi,\psi}$. To derive $\mathcal{J}_{\text{MAC},\varphi,\psi}$, let us write the first order perturbation of (13) as

$$\Delta \text{MAC} = \frac{\Delta(\varphi^H \psi \psi^H \varphi)}{\varphi^H \varphi \psi^H \psi} - \frac{\varphi^H \psi \psi^H \varphi}{(\varphi^H \varphi \psi^H \psi)^2} \Delta(\varphi^H \varphi \psi^H \psi). \quad (16)$$

Since both the φ and ψ are column vectors the product $\varphi^H \psi$ is a complex scalar. Expressing the first term from (16) it holds

$$\Delta(\varphi^H \psi \psi^H \varphi) = \Delta(\varphi^H) \psi \psi^H \varphi + \varphi^H \Delta(\psi) \psi^H \varphi + \varphi^H \psi \Delta(\psi^H) \varphi + \varphi^H \psi \psi^H \Delta(\varphi). \quad (17)$$

The terms $\Delta(\varphi^H) \psi \psi^H \varphi$ and $\varphi^H \psi \psi^H \Delta(\varphi)$ are conjugates of each other, and so are $\varphi^H \Delta(\psi) \psi^H \varphi$ and $\varphi^H \psi \Delta(\psi^H) \varphi$. Thus, it follows

$$\Delta(\varphi^H \psi \psi^H \varphi) = 2\Re(\varphi^H \Delta(\psi) \psi^H \varphi) + 2\Re(\varphi^H \psi \psi^H \Delta(\varphi)) \quad (18)$$

$$= 2\Re(\psi^H \varphi \varphi^H \Delta \psi) + 2\Re(\varphi^H \psi \psi^H \Delta \varphi). \quad (19)$$

Finally, for every complex vectors y and x the real part of the inner product writes $\Re(y^H x) = \Re((\Re(y) + i\Im(y))^H (\Re(x) + i\Im(x))) = \Re(y)^T \Re(x) + \Im(y)^T \Im(x)$, hence it holds

$$\Re(\psi^H \varphi \varphi^H \Delta \psi) = [\Re(\varphi \varphi^H \psi)^T \quad \Im(\varphi \varphi^H \psi)^T] \begin{bmatrix} \Delta \Re(\psi) \\ \Delta \Im(\psi) \end{bmatrix} \quad (20)$$

and

$$\Re(\varphi^H \psi \psi^H \Delta \varphi) = [\Re(\psi \psi^H \varphi)^T \quad \Im(\psi \psi^H \varphi)^T] \begin{bmatrix} \Delta \Re(\varphi) \\ \Delta \Im(\varphi) \end{bmatrix}. \quad (21)$$

The second term of (16) is derived with a scheme analogous to the one depicted in (17)-(21). After sorting the respective terms, the partial derivatives of the MAC with respect to the real and imaginary parts of the mode shapes are

$$\frac{\partial \text{MAC}}{\partial \Re(\varphi)} = \frac{2\Re(\psi \psi^H \varphi)^T}{\varphi^H \varphi \psi^H \psi} - \frac{\varphi^H \psi \psi^H \varphi \psi^H \psi}{(\varphi^H \varphi \psi^H \psi)^2} 2\Re(\varphi)^T \quad (22)$$

$$\frac{\partial \text{MAC}}{\partial \Im(\varphi)} = \frac{2\Im(\psi \psi^H \varphi)^T}{\varphi^H \varphi \psi^H \psi} - \frac{\varphi^H \psi \psi^H \varphi \psi^H \psi}{(\varphi^H \varphi \psi^H \psi)^2} 2\Im(\varphi)^T \quad (23)$$

and

$$\frac{\partial \text{MAC}}{\partial \Re(\psi)} = \frac{2\Re(\varphi \varphi^H \psi)^T}{\varphi^H \varphi \psi^H \psi} - \frac{\varphi^H \psi \psi^H \varphi \varphi^H \varphi}{(\varphi^H \varphi \psi^H \psi)^2} 2\Re(\psi)^T \quad (24)$$

$$\frac{\partial \text{MAC}}{\partial \Im(\psi)} = \frac{2\Im(\varphi \varphi^H \psi)^T}{\varphi^H \varphi \psi^H \psi} - \frac{\varphi^H \psi \psi^H \varphi \varphi^H \varphi}{(\varphi^H \varphi \psi^H \psi)^2} 2\Im(\psi)^T. \quad (25)$$

Combining (22)-(25) to the analytical sensitivity $\mathcal{J}_{\text{MAC},\varphi,\psi}$ after (15), the covariance of the MAC writes

$$\text{cov}(\text{MAC}) = \mathcal{J}_{\text{MAC},\varphi,\psi} \Sigma_{\varphi,\psi} \mathcal{J}_{\text{MAC},\varphi,\psi}^T.$$

4 Application

The presented scheme for the uncertainty computation is tested on a numerical simulation of a 6 degree of freedom (DOF) spring mass system in a Monte Carlo (MC) setup with 1000 simulations. The following application directly refers to the one in [6] that validated the variance estimation of natural frequencies and damping ratios in such a framework. In addition to the uncertainty quantification of MAC, this paper validates variance estimation for the mode shape computation. The chain-like system is excited with a white noise signal in all DOFs with sampling frequency of 50Hz for 2000 seconds and the responses are measured at 1, 2 and 5 DOF. Gaussian white noise with 5% of the standard deviation of the output is added to the response at each channel. The influence of the two underlying mode shape normalization cases, depicted in (7) and (8), on the variance computation is investigated.

Both the output-only data driven subspace-based system identification with the unweighted principal component (SSI-UPC) and the variance computation in the corresponding framework are set up with a single system order of 12, time lags of 15 and 200 blocks for the covariance computation of the data Hankel matrix. Six modes are tracked in each simulation. In both mode shape normalization cases the second component of the mode shape vector was selected for the normalization. The exact and calculated means of the real parts of the identified mode shapes with the respective Coefficients of Variation (CV) are depicted in Table 1 and Table 2.

DOF/Case		1	2	3	4	5	6
DOF ₁	Exact	0.6834	0.8414	1.3228	-1.7442	-1.0222	-0.7374
	Mean MC	0.6826	0.8413	1.3226	-1.7428	-1.0220	-0.7380
	CV[%]	1.241	0.240	0.368	1.927	0.523	1.270
DOF ₂	Exact	1	1	1	1	1	1
	Mean MC	1	1	1	1	1	1
	CV[%]	0	0	0	0	0	0
DOF ₅	Exact	2.0962	-0.6158	0.2154	-2.5708	0.9707	-0.7207
	Mean MC	2.0957	-0.6157	0.2153	-2.5685	0.9710	-0.7204
	CV[%]	0.615	0.123	0.809	1.368	0.867	2.336

Table 1: Comparison of the exact and mean values with corresponding CV from Monte Carlo simulation of estimated mode shapes. Normalization scheme 1.

DOF/Case		1	2	3	4	5	6
DOF ₁	Exact	0.2823	0.5824	0.7911	0.5344	0.5914	0.5134
	Mean MC	0.2819	0.5824	0.7910	0.5344	0.5915	0.5134
	CV[%]	1.040	0.159	0.120	0.977	0.389	1.429
DOF ₂	Exact	0.4131	0.6922	0.5980	-0.3066	-0.5786	-0.6963
	Mean MC	0.4131	0.6922	0.5980	-0.3064	-0.5786	-0.6962
	CV[%]	0.2819	0.5824	0.7910	0.5344	0.5915	0.5134
DOF ₅	Exact	0.8659	-0.4262	0.1288	0.7877	-0.5616	0.5018
	Mean MC	0.8659	-0.4262	0.1288	0.7870	-0.5614	0.5013
	CV[%]	0.144	0.116	0.661	0.797	0.605	1.995

Table 2: Comparison of exact and mean values with corresponding CV from Monte Carlo simulation of estimated mode shapes. Normalization scheme 2.

Both Table 1 and Table 2 reveal that calculated MC means are close to the exact values of the mode shapes, with the highest CV of 2.336% for mode 6. A comparison between the standard deviations of the mode shape components computed from the MC simulation, σ_{MC} , and the mean standard deviations from the perturbation theory (PT), σ_{PT} is depicted in Table 3 and Table 4.

DOF/Case	Standard deviation of $\Re(\phi)$ [$\cdot 10^{-2}$]						Standard deviation of $\Im(\phi)$ [$\cdot 10^{-2}$]						
	1	2	3	4	5	6	1	2	3	4	5	6	
DOF ₁	σ_{PT}	0.85	0.21	0.47	3.40	0.54	0.95	0.84	0.24	0.51	3.47	0.54	0.92
	σ_{MC}	0.84	0.20	0.46	3.52	0.53	0.97	0.80	0.23	0.51	3.50	0.54	0.91
DOF ₂	σ_{PT}	0.00	0.00	0.00	0.00	0.00	0.00	0.00	0.00	0.00	0.00	0.00	0.00
	σ_{MC}	0.00	0.00	0.00	0.00	0.00	0.00	0.00	0.00	0.00	0.00	0.00	0.00
DOF ₅	σ_{PT}	1.38	0.08	0.17	8.77	0.87	1.69	1.44	0.13	0.20	8.85	0.88	1.75
	σ_{MC}	1.27	0.07	0.17	8.97	0.88	1.67	1.32	0.12	0.19	9.01	0.86	1.79

Table 3: Standard deviations of real and imaginary part of the mode shapes from perturbation approach and Monte Carlo simulations. Normalization scheme 1.

DOF/Case	Standard deviation of $\Re(\phi)$ [$\cdot 10^{-2}$]						Standard deviation of $\Im(\phi)$ [$\cdot 10^{-2}$]						
	1	2	3	4	5	6	1	2	3	4	5	6	
DOF ₁	σ_{PT}	0.30	0.09	0.10	0.53	0.23	0.74	0.35	0.17	0.31	1.06	0.31	0.64
	σ_{MC}	0.30	0.09	0.10	0.55	0.23	0.73	0.33	0.17	0.30	1.06	0.32	0.65
DOF ₂	σ_{PT}	0.22	0.06	0.14	0.81	0.22	0.29	0.00	0.00	0.00	0.00	0.00	0.00
	σ_{MC}	0.21	0.06	0.14	0.82	0.22	0.29	0.00	0.00	0.00	0.00	0.00	0.00
DOF ₅	σ_{PT}	0.14	0.05	0.08	0.65	0.34	1.01	0.30	0.09	0.10	0.53	0.23	0.74
	σ_{MC}	0.13	0.05	0.08	0.66	0.34	0.99	0.30	0.09	0.10	0.53	0.23	0.74

Table 4: Standard deviations of real and imaginary part of the mode shapes from perturbation approach and Monte Carlo simulations. Normalization scheme 2.

Both Table 3 and Table 4 illustrate that the differences between the standard deviations obtained from the MC simulations and the mean standard deviations computed using perturbation theory (PT) are negligible. Higher standard deviations, on average, of all DOFs in Table 3 correspond to higher mean values of the mode shape components in Table 1. That results in a small differences between the CV of estimated DOFs which is illustrated, for the two normalization schemes, in Table 1 and Table 2 respectively.

Results presented so far were computed for a single sample size N , which, naturally, is the case when using such framework for uncertainty quantification in real-life applications. That, however, should hold for any sufficient data length. Analyzing results computed on different sample lengths provide arguments for deploying such framework and allow to draw some conclusions about the distribution properties of the estimated mode shapes. For that purpose introduce some variables that depend on standard deviations of $\Re(\phi)$ and $\Im(\phi)$ computed from the MC simulations such as

$$\begin{aligned}
\sigma_{\Re(\phi_{r,i})_{MC}} &= \sqrt{\text{var}(\Re(\phi_{r,i}))}, & \sigma_{\Im(\phi_{r,i})_{MC}} &= \sqrt{\text{var}(\Im(\phi_{r,i}))}, \\
\bar{\sigma}_{\Re(\phi)_{MC}} &= \sum_{r=1}^3 \sum_{i=1}^6 \sigma_{\Re(\phi_{r,i})_{MC}}, & \bar{\sigma}_{\Im(\phi)_{MC}} &= \sum_{r=1}^3 \sum_{i=1}^6 \sigma_{\Im(\phi_{r,i})_{MC}}, \\
\alpha_{\Re(\phi)_{MC}} &= \bar{\sigma}_{\Re(\phi)_{MC}} \sqrt{N}, & \alpha_{\Im(\phi)_{MC}} &= \bar{\sigma}_{\Im(\phi)_{MC}} \sqrt{N}.
\end{aligned} \tag{26}$$

The $r = 1 \dots 3$ denotes the number of measured DOF, $i = 1 \dots 6$ denotes the number of identified modes and the $j = 1 \dots MC$, where $MC = 1000$ and j denotes the j -th Monte Carlo simulation. Now, recall that proposed perturbation approach computes variance of the real and imaginary parts of the mode shape component, $\sigma_{\Re(\phi_{r,i})_{PT,j}}$ and $\sigma_{\Im(\phi_{r,i})_{PT,j}}$, for a single realization j , hence 1000 simulations enable to compute

the variance of $\sigma_{\Re(\phi_{r,i})_{PT}}$ and $\sigma_{\Im(\phi_{r,i})_{PT}}$ which, for the variables formulated in (26), writes

$$\begin{aligned}\bar{\sigma}_{\Re(\phi)_{PT}} &= \frac{1}{MC} \sum_{r=1}^3 \sum_{i=1}^6 \sum_{j=1}^{MC} \sigma_{\Re(\phi_{r,i})_{PT,j}}, & \bar{\sigma}_{\Im(\phi)_{PT}} &= \frac{1}{MC} \sum_{r=1}^3 \sum_{i=1}^6 \sum_{j=1}^{MC} \sigma_{\Im(\phi_{r,i})_{PT,j}}, \\ \sigma^*_{\Re(\phi)_{PT}} &= \sum_{r=1}^3 \sum_{i=1}^6 \sqrt{\text{var}(\sigma_{\Re(\phi_{r,i})_{PT}})}, & \sigma^*_{\Im(\phi)_{PT}} &= \sum_{r=1}^3 \sum_{i=1}^6 \sqrt{\text{var}(\sigma_{\Im(\phi_{r,i})_{PT}})}, \\ \alpha_{\Re(\phi)_{PT}} &= \bar{\sigma}_{\Re(\phi)_{PT}} \sqrt{N}, & \alpha_{\Im(\phi)_{PT}} &= \bar{\sigma}_{\Im(\phi)_{PT}} \sqrt{N}.\end{aligned}\quad (27)$$

Analysis of the variables in (26) and (27) computed on the data sets with different sample lengths is depicted on Figure 1.

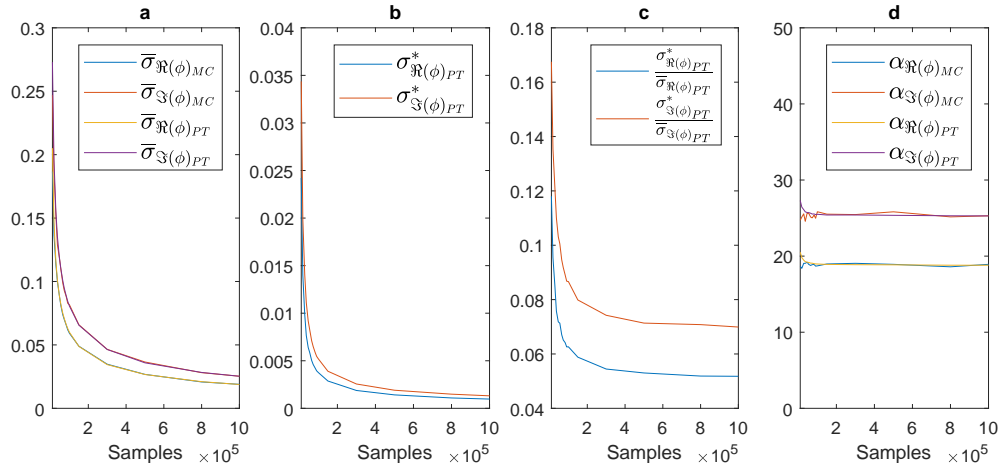


Figure 1: Sum of standard deviations of the mode shape components from Monte Carlo simulation and mean perturbation theory depending on number of samples (a). Standard deviation of the sum of standard deviations of the mode shape components from Monte Carlo simulation and mean perturbation theory (b). CV of the standard deviation of mode shape components from perturbation theory depending on number of samples (c). Sum of standard deviations of the mode shape components from Monte Carlo simulation and mean perturbation theory scaled with a square root of corresponding data length (d). Normalization 1.

Since mode shapes estimates are converging to their true value the $\bar{\sigma}_{\Re(\phi)_{MC}}$, $\bar{\sigma}_{\Im(\phi)_{MC}}$, $\bar{\sigma}_{\Re(\phi)_{PT}}$ and $\bar{\sigma}_{\Im(\phi)_{PT}}$ are converging to zero, which is illustrated in the 'a' part of Figure 1. The 'b' part shows that the errors in the perturbation approach converge to zero. The CVs $\sigma^*_{\Re(\phi)_{PT}}/\bar{\sigma}_{\Re(\phi)_{PT}}$ and $\sigma^*_{\Im(\phi)_{PT}}/\bar{\sigma}_{\Im(\phi)_{PT}}$ converge to a constant value of 5.5% and 7.5% respectively, see 'c' part of Figure 1, which illustrates that the relative error summed from all the mode shape components for selected model order n is very small. That also arguments for using the proposed framework while having just one measurement set. The 'd' part of Figure 1 illustrates that the pairs $\bar{\sigma}_{\Re(\phi)_{PT}}$ and $\bar{\sigma}_{\Re(\phi)_{MC}}$ with $\bar{\sigma}_{\Im(\phi)_{PT}}$ and $\bar{\sigma}_{\Im(\phi)_{MC}}$ converge with rate of order \sqrt{N} to a similar constant, which also justifies estimating the variance of the mode shape components with the perturbation approach.

The MAC values computed between the mode shapes estimated at model order 6 from one arbitrary data set are depicted on Figure 2.

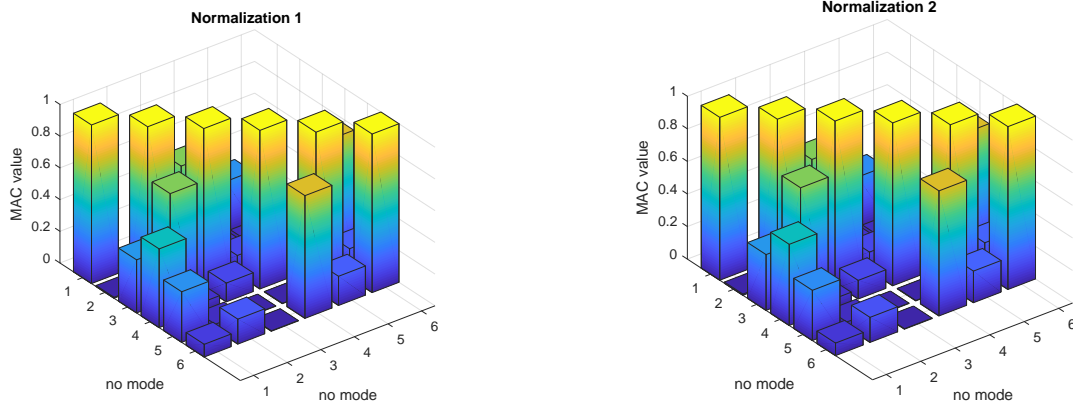


Figure 2: MAC values computed for one simulation. Normalization scheme 1 (left) and normalization scheme 2 (right).

As shown in (14) the diagonal of the MAC matrix plotted in Figure 2 is equal to one. The histograms of selected MAC values obtained from MC simulations with the corresponding standard deviations computed using the perturbation approach are depicted on Figure 3 and Figure 4 respectively.

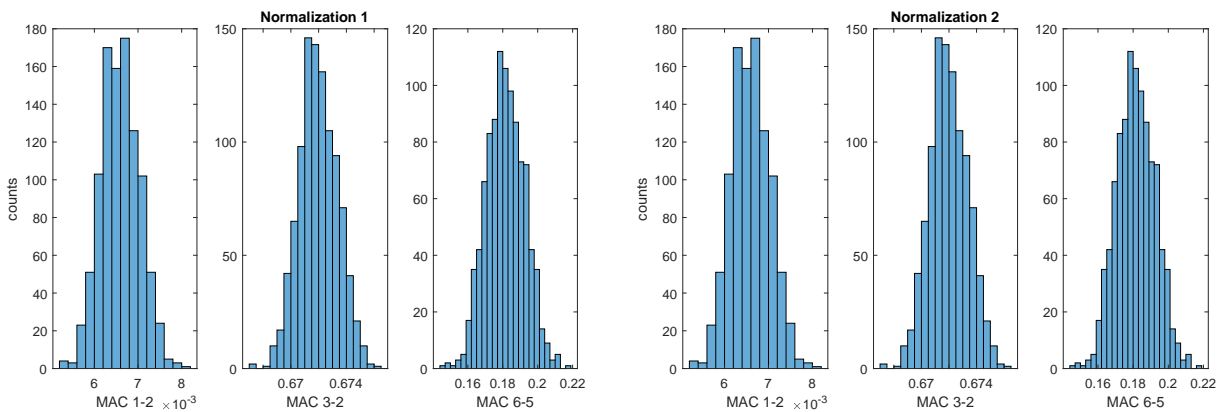


Figure 3: Selected histograms of MAC from Monte Carlo simulations.

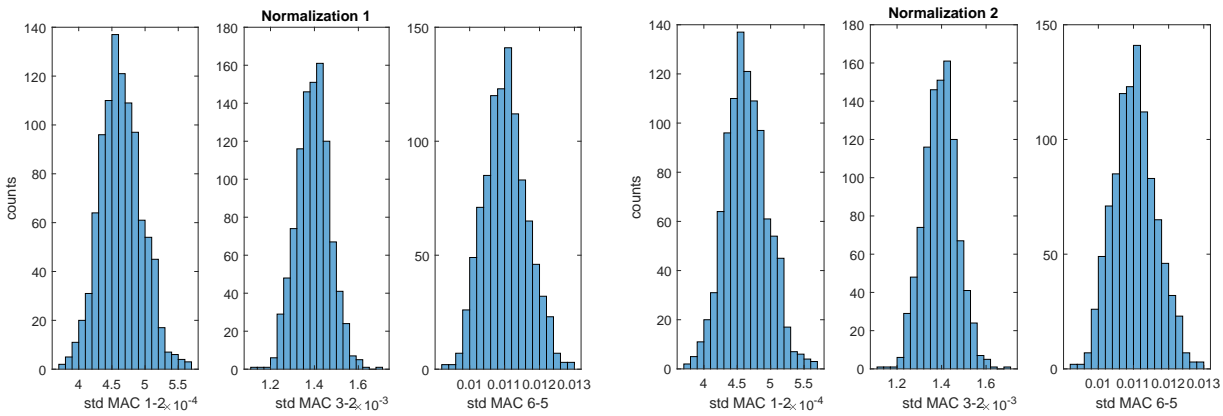


Figure 4: Selected histograms of standard deviations of MAC computed with perturbation approach.

The histograms illustrate the validity of Gaussian approximation of MAC stated by CLT in (9). In addition,

tion, the MAC values and the standard deviations of MAC for both normalization schemes are numerically identical, hence render its computation invariant towards the normalization of the mode shape. The standard deviations of the MAC obtained from the MC simulations and the mean standard deviations computed using the PT are presented in Table 5.

		Standard deviation of MAC [$\cdot 10^{-2}$]											
Mode/Case		Normalization scheme 1						Normalization scheme 2					
		1	2	3	4	5	6	1	2	3	4	5	6
1	σ_{PT}	-	0.05	0.30	1.09	0.42	0.49	-	0.05	0.30	1.09	0.42	0.49
	σ_{MC}	-	0.04	0.28	1.11	0.42	0.49	-	0.04	0.28	1.11	0.42	0.49
2	σ_{PT}	0.05	-	0.14	0.14	0.10	0.59	0.05	-	0.14	0.14	0.10	0.59
	σ_{MC}	0.04	-	0.14	0.14	0.10	0.58	0.04	-	0.14	0.14	0.10	0.58
3	σ_{PT}	0.30	0.14	-	0.24	0.03	0.05	0.30	0.14	-	0.24	0.03	0.05
	σ_{MC}	0.28	0.14	-	0.23	0.03	0.05	0.28	0.14	-	0.23	0.03	0.05
4	σ_{PT}	1.09	0.14	0.24	-	0.13	1.06	1.09	0.14	0.24	-	0.13	1.06
	σ_{MC}	1.11	0.14	0.23	-	0.13	1.08	1.11	0.14	0.23	-	0.13	1.08
5	σ_{PT}	0.42	0.10	0.03	0.13	-	1.10	0.42	0.10	0.03	0.13	-	1.10
	σ_{MC}	0.42	0.10	0.03	0.13	-	1.09	0.42	0.10	0.03	0.13	-	1.09
6	σ_{PT}	0.49	0.59	0.05	1.06	1.10	-	0.49	0.59	0.05	1.06	1.10	-
	σ_{MC}	0.49	0.58	0.05	1.08	1.09	-	0.49	0.58	0.05	1.08	1.09	-

Table 5: Standard deviations of MAC values for both normalization schemes for perturbation approach and Monte Carlo simulations.

It can be observed that the differences between the standard deviations of MAC computed from MC simulations and the mean ones obtained from the perturbation approach are small. The influence of data length on the standard deviations of MAC computed from MC simulations and the mean standard deviations obtained from the PT is illustrated in Figure 5.

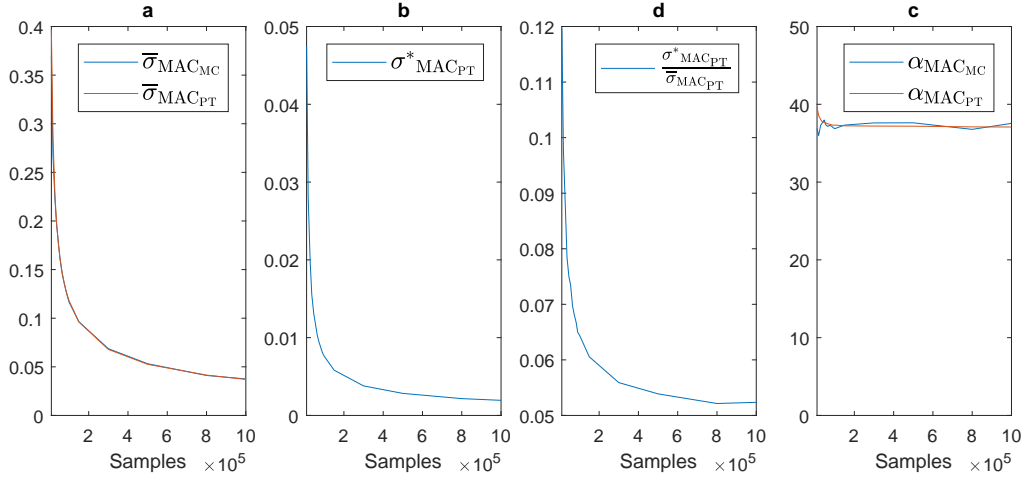


Figure 5: Sum of standard deviations of MAC from Monte Carlo simulation and mean perturbation theory depending on number of samples (a). Standard deviation of the sum of standard deviations of MAC from Monte Carlo simulation and mean perturbation theory (b). CV of the standard deviation of MAC from perturbation theory (c). Sum of standard deviations of MAC from Monte Carlo simulation and mean perturbation theory scaled with a square root of corresponding data length (d). Normalization 1.

The parameters used in this analysis follow a similar notation as in the case of mode shape uncertainties, see (26) and (27). The 'a' part of Figure 5 illustrates that the $\bar{\sigma}_{MAC_{MC}}$ and $\bar{\sigma}_{MAC_{PT}}$ are converging to zero. In addition, note that there is no visible difference between the results from MC simulations and

the mean ones obtained from PT. Second, the errors in the variance estimates of MAC computed with the perturbation approach, $\sigma^*_{\text{MAC}_{\text{PT}}}$, also converge to zero, which is presented in the 'b' part of Figure 5. The CV of the standard deviations of MAC, $\sigma^*_{\text{MAC}_{\text{PT}}}/\bar{\sigma}_{\text{MAC}_{\text{PT}}}$, computed using perturbation approach converge to a constant value of 5.2%, see 'c' part of Figure 5, which, like in the case of mode shape uncertainties, is small and arguments for using proposed framework while having just one measurement set. Lastly, the 'd' part of Figure 5 illustrates that both the $\bar{\sigma}_{\text{MAC}_{\text{MC}}}$ and $\bar{\sigma}_{\text{MAC}_{\text{PT}}}$ converges with rate \sqrt{N} to a similar constant.

5 Conclusions

This paper presented an approach to quantify the statistical uncertainty of MAC computed between different mode shape vectors. Proposed method was verified against Monte Carlo simulations of a simple chain system where the resulting differences between two frameworks were negligible, as expected. Uncertainty quantification was found invariant towards the underlying schemes for mode shape normalization, as expected. Theoretical asymptotic properties of MAC were validated with simulations with increasing sample size. The future work will consist of real-life application of both the uncertainty quantification of mode shapes and MAC, through its implementation in the future release of the ARTEMIS MODAL PRO [8] software.

References

- [1] M. Döhler, P. Andersen, and L. Mevel. Variance computation of modal parameter estimates from upc subspace identification. In *IOMAC - 7th International Operational Modal Analysis Conference*, Ingolstadt, Germany, 2017.
- [2] M. Döhler, X.-B. Lam, and L. Mevel. Uncertainty quantification for modal parameters from stochastic subspace identification on multi-setup measurements. *Mechanical Systems and Signal Processing*, 36:562–581, 04 2013.
- [3] M. Döhler and L. Mevel. Fast multi-order computation of system matrices in subspace-based system identification. *Control Engineering Practice*, 20(9):882 – 894, 2012.
- [4] M. Döhler and L. Mevel. Efficient multi-order uncertainty computation for stochastic subspace identification. *Mechanical Systems and Signal Processing*, 38(2):346–366, 2013.
- [5] R. J. Allemang. The modal assurance criterion (MAC): Twenty years of use and abuse. *Journal of Sound and Vibration*, 37, 01 2003.
- [6] P. Mellinger, M. Döhler, and L. Mevel. Variance estimation of modal parameters from output-only and input/output subspace-based system identification. *Journal of Sound and Vibration*, 379(Supplement C):1 – 27, 2016.
- [7] E. Reynders, R. Pintelon, and G. D. Roeck. Uncertainty bounds on modal parameters obtained from stochastic subspace identification. *Mechanical Systems and Signal Processing*, 22(4):948 – 969, 2008. Special Issue: Crack Effects in Rotordynamics.
- [8] Structural-Vibration-Solutions-A/S. ARTEMIS MODAL PRO 6.0. In <http://svibs.com>, 2018.
- [9] P. van Overschee and B. de Moor. *Subspace Identification for Linear Systems*. Springer, 1st edition, 1996.